Turkish Journal of Physics

http://journals.tubitak.gov.tr/physics/

Research Article

Turk J Phys
(2021) 45: 26 – 42

doi:10.3906/fiz-2003-5

Modeling and parametric study of dielectric barrier discharge in pure nitrogen at atmospheric pressure

Mohammed Habib Allah LAHOUEL*, Djilali BENYOUCEF, Hocine TEBANI
Electrical Engineering and Renewable Energy Laboratory, Hassiba Benbouali University of Chlef, Ouled Fares, Chlef, Algeria

Received: 06.03.2020 • **Accepted/Published Online:** 18.01.2021 • **Final Version:** 27.02.2021

Abstract: This paper presents the one-dimensional simulation of the dielectric barrier discharge (DBD) in pure nitrogen at atmospheric pressure using a sinusoidal supply, within a reactor which consists of two parallel plates. For this purpose, significant reactions among the reactive species in the discharge are taken into account in this work by considering more than 70 reactions for 13 species. The model used in this study to describe the kinetics of the plasma species is the second order fluid model which consists in replacing the Boltzmann equation by these first three moments by using the drift-diffusion approximation for flux. In order to validate the model developed in this research, a comparison of the simulated discharge currents obtained with available experimental data is carried out, before presenting the evolution of the properties of the plasma species. After that, a parametric study is performed showing the effect of some parameters like applied voltage, frequency and nature of the coating dielectric material on the characteristics of DBD in nitrogen. Simulation results for a double dielectric DBD reactor are also presented at the end of this paper.

Key words: Fluid model, dielectric barrier discharge; nitrogen plasma; atmospheric pressure

1. Introduction

Due to their importance in many technological developments, atmospheric pressure dielectric barrier discharges (DBD) have attracted much attention from researchers over the past decades in various industrial applications such as:

Ozone generation: The first and most important application of DBD is the generation of ozone from the treatment of air or oxygen. The synthesis of ozone in DBD is carried out by chemical reaction. While the purification of drinking water remains the most important ozone market, other applications have emerged.

Gas treatment: DBD is studied in the destruction of toxic exhaust gases, such as carbon monoxide CO, nitrogen oxides NOx and in the reduction of greenhouse gas emissions, such as carbon dioxide (CO2), responsible for global warming.

Surface modification: One of the main properties of DBDs is that they can operate under filamentous or homogeneous conditions. The ”homogeneous” characteristic gives them the property of being able to act for a uniform modification of the treated surfaces.

This leads to the need for a better understanding of the behavior of this type of plasma experimentally and theoretically [1,2].

This type of discharge can easily be arced; It is therefore the simplest way to produce a cold plasma,

*Correspondence: habib221@live.com

the DBD are formed between two metal electrodes in parallel, one or two of them are covered with dielectric material to ensure the limitation of the current during the discharge [3,4].

According to previous research, during the creation of cold plasma, a large chemical process present in gas, formation of active species by collision of electrons with neutrals, formation of species in a metastable state (long-lived species of life), surface reactions, etc.

Numerical modeling is a very useful tool for studying the behavior of DBDs and their optimization with a view to using them in industrial applications. In recent years, DBD modeling has developed rapidly, whether in pure gases [5] or in gas mixtures [6].

Nitrogen plasma is the basis for the development of several industrial applications, such as the cutting and nitriding of metals to improve surface hardness [7,8]. The development of such DBD applications requires a better understanding of the chemical and physical processes of plasma. This involves the use of appropriate models to achieve optimal results.

Nitrogen plasma produced in DBDs at atmospheric pressure has been classified into two forms of discharge, homogeneous and filamentary [5]. Previous studies have shown variations in the characteristics of nitrogen plasma, with various mechanisms of electron emission, but their results have not resolved the plasma processes. In this study, a simulation of the behavior of the discharge is carried out according to the state of the newly created species by varying the different parameters used for the creation of this type of plasma.

The one-dimensional model used for the simulation of DBD in nitrogen considers the most important chemical reactions from reliable and revised previous studies. The results of the calculations obtained are compared with the available experimental data [9].

2. Numerical model

To describe the kinetics of the particles in the type of discharge object of our study, we used the fluid model which consists in replacing the Boltzmann equation by these moments using the drift diffusion approximation [10], these equations are described below [11].

The particle continuity equation is given by:

$$\frac{\partial n_{e,i,n}}{\partial t} + \nabla . \ _{e,i,n} = S_{e,i,n} \ , \tag{1}$$

$$S_{e,i,n} = \sum_{j=1}^{M} c_{j,e} R_j \ , \tag{2}$$

$$_{e,i} = \mu_{e,i} E n_{e,i} - D_{e,i} \nabla n_{e,i}, \tag{3}$$

$$_{n} = -D_n \nabla n_n, \tag{4}$$

where the indicators e, i and n refer to electrons, ions and neutrals, respectively. With n_e, n_i and n_n are the number densities. $_e$, $_i$ and $_n$ are the particles flux of electron, ion, and neutrals respectively. $S_{e,i,n}$ is the production or loss rate for every species in each chemical interaction occur in discharge. $c_{j,e}$ represent stoichiometric number of electrons j, R_j the reaction rate and M is the number of electron reactions. E is the electric field, $D_{e,i}$ and $\mu_{e,i}$ are the diffusion coefficient and mobility of electron and ions, respectively.

The electron energy equation is given by:

$$\frac{\partial n_\varepsilon}{\partial t} + \nabla . \ _\varepsilon + E . \ _e = S_\varepsilon \ . \tag{5}$$

The flux including source expression settled as [12]:

$$_\varepsilon = -\mu_e E n_\varepsilon - D_e \nabla n_\varepsilon, \tag{6}$$

where ε refers to energy, with n_ε is the electron energy density, S_ε : energy loss or production by inelastic collisions.

$$S_\varepsilon = -e \ _e . E - \sum_{j=1}^{P} c_{j,e} R_j \varepsilon_j \tag{7}$$

P is the number of inelastic collisions, the energy lost or produced in a collision represented by ε_j which is considered similar to the threshold of a reaction. In the previous expressions, the source coefficients specified through the system stoichiometry, using rate coefficients [13].

$$-\nabla . \varepsilon_0 . \varepsilon_r \nabla V = \rho_q \ , \tag{8}$$

with ε_0 is the vacuum permittivity and ε_r is the relative permittivity. ρ_q is the space charge density

$$\rho_q = q \left(\sum_{k=1}^{N} Z_k n_k - n_e \right) \tag{9}$$

q is the absolute value of electronic charge, Z_k is the electric charge, E is the electric field and V is the electric potential.

The properties of the dielectric are described by the following relation [13]:

$$D = \varepsilon_0 \varepsilon_r E. \tag{10}$$

2.1. Boundary conditions:

The impact of heavy species on the surface of the dielectric barrier represents the most important parameter governing the behavior of the discharge.

1. The accumulation of charges on the surface of the dielectric, resulting from variations in the flows of electrons and ions is described as follows [10]:

$$-n. (D_1 - D_2) = \rho_s, \tag{11}$$

$$\frac{d\rho_s}{dt} = n.J_i + n.J_e \ , \tag{12}$$

with ρ_s is the density of surface charge.

On the boundaries, the electric fields displacement is defined by D_1 and D_2.

$n.J_i$: the total current density of ion, and $n.J_e$: the total current density of electron.

1. At electrode surface, the electron energy is written as [14]:

$$_{\varepsilon}.\mathbf{n} = \frac{1}{3} v_{e,th} \overline{\varepsilon} n_e, \tag{13}$$

where $\mathbf{n}$ is boundary normal vector, $v_{e,th}$ is electron thermal, and $\overline{\varepsilon}$ is the mean energy of electron.

1. For electron, electron energy, and heavy species beside to both sides of the gap, the boundaries conditions are written as [15]:

$$\begin{cases} -\mathbf{n}._{e} = 0 \\ -\mathbf{n}._{\varepsilon} = 0 \\ -\mathbf{n}._{k} = 0 \end{cases} \tag{14}$$

Surface reactions neutralize ions, at the scale of dielectric surfaces, the surface interaction coefficient is used, specifying the perspective of a species that will react on the surface [16], this is described mathematically by the relation below:

$$_{k}.\mathbf{n} = \frac{\beta_k}{4} \sqrt{\frac{8 k_B T_k}{\pi m_k}} n_k, \tag{15}$$

where k refers to heavy species, β_k is the surface interaction coef?cient, k_B Boltzmann's constant, T_k and m_k are respectively the temperature and the mass of heavy species.

3. Plasma chemistry

In our study, we took into account 13 species: $(electron, N, N^+, N_2, N_2^+, N_3^+, N_4^+, N_2(A^3\sum_u^+), N_2(B^3\prod g), N_2(C^3\prod u), N_2(a^{'1}\sum_u^-),\ N(P), N(D))$ including 71 reactions: dissociation and ionization; recombination processes, neutrals-neutrals reactions; three-body reactions, excitation and deexcitation. All the processes mentioned are gathered in Table, each reaction is characterized by its rate coefficient.

Table. Reaction set for nitrogen.

No.	Reaction	Threshold	Rate coefficient [m^3/s.mol or m^6/s.mol(*) or 1/s(**)]	Ref.
1	$e + N_2^+ \rightarrow N + N(P)$	0.00	$0.11 \times 1.75 \times 10^{-13} \times (0.026/T_e)^{0.3}$	[21]
2	$e + N_2^+ \rightarrow N + N(D)$	0.00	$0.37 \times 1.75 \times 10^{-13} \times (0.026/T_e)^{0.3}$	[21]
3	$e + N_2^+ \rightarrow N(D) + N(D)$	0.00	$0.52 \times 1.75 \times 10^{-13} \times (0.026/T_e)^{0.3}$	[21]
4	$e + N_4^+ \rightarrow N_2\left(C^3\prod u\right) + N_2$	0.00	$2 \times 10^{-12} \times (300/Te)^{0.5}$	[10]
5	$e + N_3^+ \rightarrow N_2 + N$	0.00	$2 \times 10^{-13} \times (0.026/Te)^{0.5}$	[2]
6	$e + N_2 \rightarrow e + N_2$	0.00	Cross section	*
7	$e + N_2 \rightarrow e + N_2$	0.02	Cross section	*
8	$e + N_2 \rightarrow e + N_2$	0.29	Cross section	*
9	$e + N_2 \rightarrow e + N_2$	0.29	Cross section	*
10	$e + N_2 \rightarrow e + N_2$	0.59	Cross section	*
11	$e + N_2 \rightarrow e + N_2$	0.88	Cross section	*
12	$e + N_2 \rightarrow e + N_2$	1.17	Cross section	*
13	$e + N_2 \rightarrow e + N_2$	1.47	Cross section	*

Table. (Continued).

No.	Reaction	Threshold	Rate coefficient [m^3/s.mol or m^6/s.mol(*) or 1/s(**)]	Ref.
14	$e + N_2 \rightarrow e + N_2$	1.76	Cross section	*
15	$e + N_2 \rightarrow e + N_2$	2.06	Cross section	*
16	$e + N_2 \rightarrow e + N_2$	2.35	Cross section	*
17	$e + N_2 \rightarrow e + N_2(A^3 \sum_u^+)$	6.17	Cross section	*
18	$e + N_2 \rightarrow e + N_2(A^3 \sum_u^+)$	7.00	Cross section	*
19	$e + N_2 \rightarrow e + N_2(B^3 \prod g)$	7.35	Cross section	*
20	$e + N_2 \rightarrow e + N_2$	7.36	Cross section	*
21	$e + N_2 \rightarrow e + N_2(A^3 \sum_u^+)$	7.80	Cross section	*
22	$e + N_2 \rightarrow e + N_2$	8.16	Cross section	*
23	$e + N_2 \rightarrow e + N_2(a^{'1} \sum_u^-)$	8.40	Cross section	*
24	$e + N_2 \rightarrow e + N_2$	8.55	Cross section	*
25	$e + N_2 \rightarrow e + N_2$	8.89	Cross section	*
26	$e + N_2 \rightarrow e + N_2 \left(C^3 \prod u\right)$	11.03	Cross section	*
27	$e + N_2 \rightarrow e + N_2$	11.87	Cross section	*
28	$e + N_2 \rightarrow e + N + N(D)$	12.14	Cross section	*
29	$e + N_2 \rightarrow e + N_2$	12.25	Cross section	*
30	$e + N_2 \rightarrow e + N + N(P)$	13.33	Cross section	*
31	$e + N_2 \rightarrow e + e + N_2^+$	15.60	Cross section	*
32	$e + N_2 \rightarrow e + e + N + N^+$	24.34	Cross section	*
33	$e + N_2(A^3 \sum_u^+) \rightarrow e + e + N_2^+$	9.43	Cross section	[18]
34	$e + N_2(B^3 \prod g) \rightarrow e + e + N_2^+$	8.25	Cross section	[18]
35	$e + N_2 \left(C^3 \prod u\right) \rightarrow e + e + N_2^+$	4.57	Cross section	[18]
36	$e + N_2(a^{'1} \sum_u^-) \rightarrow e + e + N_2^+$	7.20	Cross section	[18]
37	$e + N \rightarrow e + N$	0.00	Cross section	*
38	$e + N \rightarrow e + N(D)$	2.38	Cross section	*
39	$e + N(D) \rightarrow e + N$	-2.38	Cross section	*
40	$e + N \rightarrow e + N(P)$	3.57	Cross section	*
41	$e + N(P) \rightarrow e + N$	-3.57	Cross section	*
42	$e + N \rightarrow e + e + N^+$	4.54	Cross section	*
43	$N_2(a^{'1} \sum_u^-) + N_2(A^3 \sum_u^+) \rightarrow N_4^+ + e$	0.00	0.25×10^{-17}	[10]
44	$N_2(a^{'1} \sum_u^-) + N_2(a^{'1} \sum_u^-) \rightarrow N_4^+ + e$	0.00	10^{-16}	[10]
45	$N + N + N_2 \rightarrow N_2 + N_2$	0.00	$8.3 \times 10^{-46} \times exp(493/T)^*$	[5]
46	$N_2(A^3 \sum_u^+) + N_2(A^3 \sum_u^+) \rightarrow N_2 \left(C^3 \prod u\right) + N_2$	0.00	1.6×10^{-16}	[10]
47	$N_2(A^3 \sum_u^+) + N_2(A^3 \sum_u^+) \rightarrow N_2(B^3 \prod g) + N_2$	0.00	3×10^{-16}	[10]
48	$N_2(A^3 \sum_u^+) + N_2 \rightarrow N_2 + N_2$	0.00	3×10^{-24}	[5]
49	$N_2(A^3 \sum_u^+) + N \rightarrow N_2 + N(P)$	0.00	$4 \times 10^{-17} * (300/T)^{0.66}$	[2]
50	$N_2(A^3 \sum_u^+) + N \rightarrow N_2 + N$	0.00	9.6×10^{-17}	[21]
51	$N_2(B^3 \prod g) + N_2 \rightarrow N_2(A^3 \sum_u^+) + N_2$	0.00	5×10^{-17}	[21]
52	$N_2(a^{'1} \sum_u^-) + N_2 \rightarrow N_2(B^3 \prod g) + N_2$	0.00	2×10^{-19}	[2]

Table. (Continued).

No.	Reaction	Threshold	Rate coefficient [m^3/s.mol or m^6/s.mol(*) or 1/s(**)]	Ref.
53	$N_2\left(C^3\prod u\right)+N_2 \rightarrow N_2(a^{'1}\sum_u^-)+N_2$	0.00	10^{-17}	[2]
54	$N(P)+N_2 \rightarrow\ N(D)+N_2$	0.00	3.3×10^{-23}	[20]
55	$N_2^+ + N_2 + N_2 \rightarrow N_4^+ + N_2$	0.00	$5.2\times10^{-41}\times(300/T)^{2.2}$*	[3]
56	$N_2^+ + N + N_2 \rightarrow N_3^+ + N_2$	0.00	$9\times10^{-42}\times exp(400/T)$*	[3]
57	$N^+ + N_2 + N_2 \rightarrow N_3^+ + N_2$	0.00	$17\times10^{-42}\times(300/T)^{2.1}$*	[3]
58	$N^+ + N + N_2 \rightarrow N_2^+ + N_2$	0.00	10^{-41}*	[3]
59	$N_2^+ + N_2(A^3\sum_u^+)\rightarrow N_3^+ + \mathrm{N}$	0.00	3×10^{-16}	[4]
60	$N_2^+ + N \rightarrow N^+ + N_2$	0.00	$7.2\times10^{-19}\times(T/300)$	[3]
60	$N_2^+ + N \rightarrow N^+ + N_2$	0.00	$7.2\times10^{-19}\times(T/300)$	[3]
61	$N_3^+ + N \rightarrow N_2^+ + N_2$	0.00	6.6×10^{-17}	[3]
62	$N_4^+ + N_2 \rightarrow N_2^+ + N_2 + N_2$	0.00	$2.1\times10^{-20}\times exp(T/121)$	[3]
63	$N_4^+ + N \rightarrow N^+ + N_2 + N_2$	0.00	10^{-17}	[3]
64	$N_2(B^3\prod g)\rightarrow N_2(A^3\sum_u^+)$	0.00	1.5×10^{5}**	[5]
65	$N_2\left(C^3\prod u\right)\rightarrow N_2(B^3\prod g)$	0.00	2.7×10^{7}**	[5]
66	$N_2(A^3\sum_u^+)\rightarrow N_2$	0.00	0.5**	[5]
67	$N_2(a^{'1}\sum_u^-)\rightarrow N_2$	0.00	100**	[5]
68	$\mathrm{N(D)+N_2\rightarrow N+N_2}$	0.00	6×10^{-21}	[21]
69	$N(P)+\mathrm{N_2}\rightarrow N+N_2$	0.00	6×10^{-20}	[21]
70	$N(D)+\ N(P)\rightarrow N_2^+ + \mathrm{e}$	0.00	$3.2\times10^{-21}\times T^{0.98}/(1-exp(-3129/T))$	[2]
71	$N\,(P)+N(P)\rightarrow N_2^+ + \mathrm{e}$	0.00	$1.92\times10^{-21}\times T^{0.98}/(1-exp(-3129/T))$	[2]

3.1. Electron impact reactions

Electrons are the most important species in plasma for their convection ability of energy; therefore, knowing trustworthy details of this process (electron-neutral scattering cross sections) is important to describe electrons kinetics in discharge plasma[1].

The cross section set for electron collisions in $\mathrm{N_2}$ used in this calculation is shown in Table, for N_2 and N taken from LXCat date base* and from [1], [2] for N_2 dissociation recombination (DR) processes. The complete set of electron impact process in this study includes 42 cross sections for N_2 and N (elastic, excitations, ionization attachment)*.

One of the most important processes in plasma chemistry is dissociative recombination. This process typically pass through two mechanisms: the direct excitation and the resonant capture in Feshbach resonances; through the dissociation, these resonances can stabilize [17].

This set of cross section contains another process, which is the stepwise ionization. This interesting process is taken into consideration in this study for four electronic states of nitrogen: $N_2(A^3\sum_u^+)$, $N_2(B^3\prod g)$, $N_2(C^3\prod u)$, $N_2(a^{'1}\sum_u^-)$, ionization by impact of electrons produces two electrons, as mentioned in Table.

[1]SIGLO database (LXCat date base) [online]. Website https://fr.lxcat.net/ [09 Febraury 2019].

The values of the total ionization cross sections are calculated using expressions given in [18].

3.2. Heavy species chemical reactions

The reactions for the production and destruction of the heavy species are shown in Table with their corresponding rate coefficients.

The reaction rate constant k^f is determined by the Arrhenius equation:

$$k^f = Ae^{-E_a/RT}, \tag{16}$$

where A is the preexponential factor, T is the temperature of the gas, E_a is the activation energy of the reaction and R is the gas constant.

Reactions (43), (44), (56), (57), (59), (74) and (73) illustrated in Table, represent associative ionization. This process has an influence on the development of discharges by metastable species [19]. The main mechanisms of loss of the metastable state are presented by reactions (43) and (44).

An important process that cannot be neglected at atmospheric pressure is the extinction of metastable states ($N_2(A^3\sum_u^+)$, $N_2(B^3\prod g)$, $N_2(C^3\prod u)$, $N_2(a^{'1}\sum_u^-)$, $N(P)$, $N(D)$); this process is taken into account by reactions of (48) to (54) and (70), (71). It is necessary to include 3 reactions for their involvement in the charge transfer process [20], which are illustrated in (45) and (55) to (58).

Reactions (64)–(67) describe the decay of ($N_2(A^3\sum_u^+)$, $N_2(B^3\prod g)$, $N_2(C^3\prod u)$, $N_2(a^{'1}\sum_u^-)$ species in the metastable state has a radiative lifespan.

4. Simulation results

In order to compare and validate the results from the model developed in this work for the simulation of the dielectric barrier discharge in pure nitrogen at atmospheric pressure which is the subject of our study, we carried out a study of this discharge under the same experimental conditions described by Bouzidi et al. [9], we considered a 1D geometry consisting of two parallel plates covered with a dielectric coating (Alumina Al_2O_3 96%) of relative permittivity $\varepsilon_r = 9$ and 0.635 mm thick. The confined space of nitrogen between the dielectric surfaces is 1mm as shown in Figure 1.

The supply voltage V of the reactor used is of sinusoidal form of frequency $f = 3\ kHz$ with a peak of $6\ kV$.

$$V = 6000 * sin(2 * \pi * f * t), \tag{17}$$

where t is the time (μs), V is the voltage applied to the electrode (A), the electrode (B) is linked to earth through a 200 Ω resistor to measure the discharge current.

The transport coefficients (mobility and diffusion) of ions are taken from [22] and [23] using the reduced mobility expression K_0 defined by:

$$K_0 = K \times (237/T_g), \tag{18}$$

where T_g is the gas temperature at which the measurement of mobility K was made.

The number density of the seed electrons assumed to be present in space is $4 \times 10^5 (1/m^3)$, of which they are distributed uniformly, with an average initial energy of 5eV, the number density of ions is assumed to be $10^5\left(1/m^3\right)$.

Figure 2 shows a comparison of the total current of the dielectric barrier discharge in Nitrogen obtained from our model and that measured [9]. From this figure, we observe a good agreement between the temporal evolution of the two currents. In fact, the current shows only one peak per alternation of the voltage and the light is radially homogeneous over the entire section of the discharge.

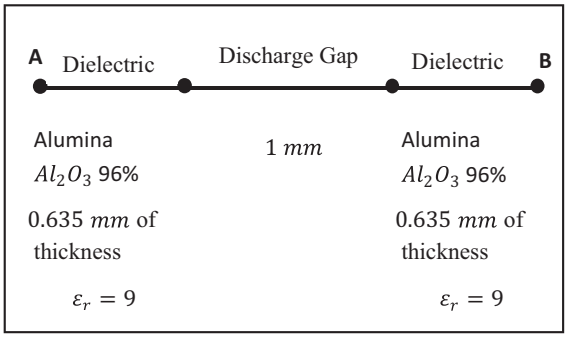

Figure 1. Geometry used in the simulation.

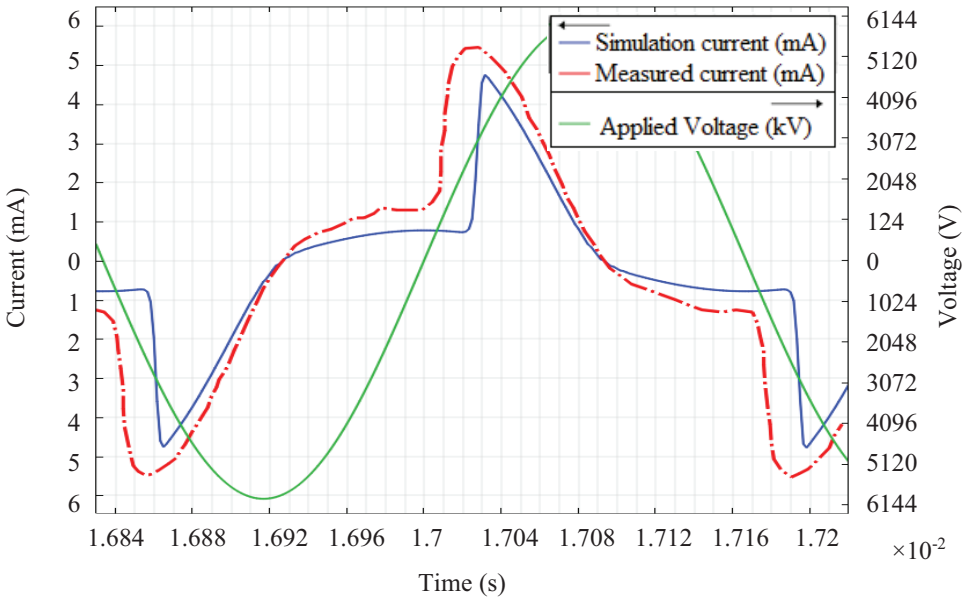

Figure 2. Comparison between the calculated and measured [9] discharge current.

The current peak moment during breakdown $t_p = 0.017$ s which we choose to take the instantaneous distributions of the different species in the plasma, leads to obtain Figure 3 for the charged species and Figure 4 for the neutral and excited species.

Figure 3 clearly shows that the ion densities are almost stable in the interelectrode space while the electron density varies between (10^6 and 10^{12}) $1/m^3$. It is a characteristic of the Townsend discharge.

The ionization and excitation collisions produced by the electron-molecule impact of nitrogen N_2 under a strong electric field, are the main causes of the increase in the densities of the ions and excited particles near the anode (see Figures 3 and 4).

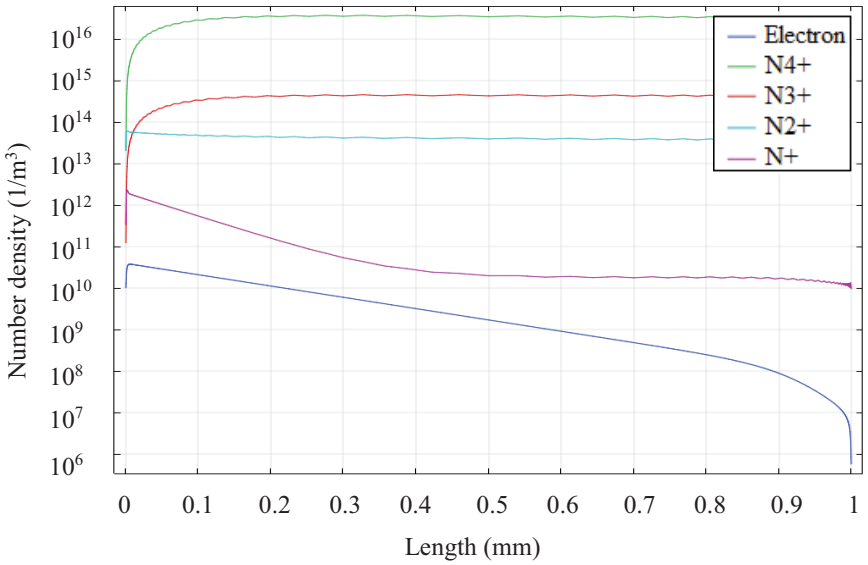

Figure 3. Spatial distributions of electronic and ionic densities at 0.017 s.

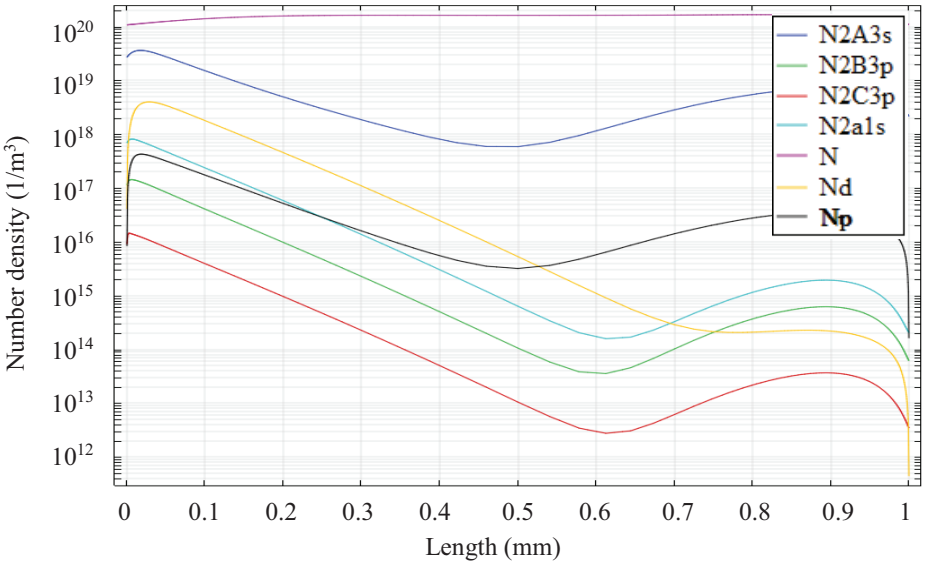

Figure 4. Spatial distributions of the densities of neutral and excited species at t = 0.017 s.

Figures 5 and 6 shows the temporal variationsof the number density of charged and neutral species respectively at the dielectric surface that cover the electrode A (Figure 1). Figure 5 shows that in positive alternate of voltage wave, the electrons number density increase by the increasing of applied voltage and its greater than other ions number densities. That is because of ionization process when electrons gain the required energy for it, for this reason we also observe the growth of ion number density. Moreover, only at the moment of breakdown (t = 0.017 s), electrons and ions number densities are the same. In the next negative alternate, we can see that the electron number density getting low when they are heading to the other boundaries of point B (Figure 1). The same manners manifest with the ions, but with a lower length for their heaviness.

$N_4{}^+$ dominate because of the associative ionization process, as mentioned in reaction (43) and (44) from Table. The dominate metastable as shown in figure 6 is between $N_2(A^3\sum_u^+)$ and $N_2(a'^1\sum_u^-)$. Also this process can produce $N_2{}^+$ as mentioned in reaction (72) and (73) ions by $N(P)$ and $N(D)$ which they dominate in discharge gap.

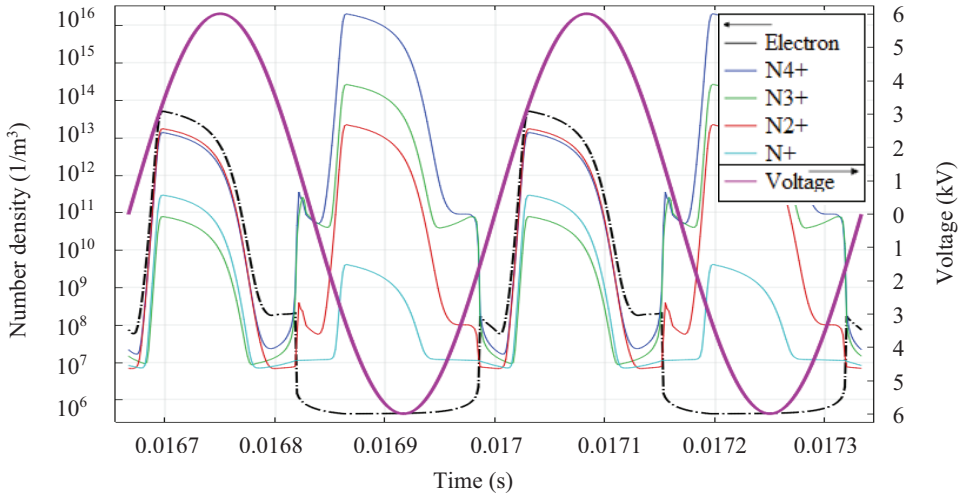

Figure 5. Temporal variation of charged species number density.

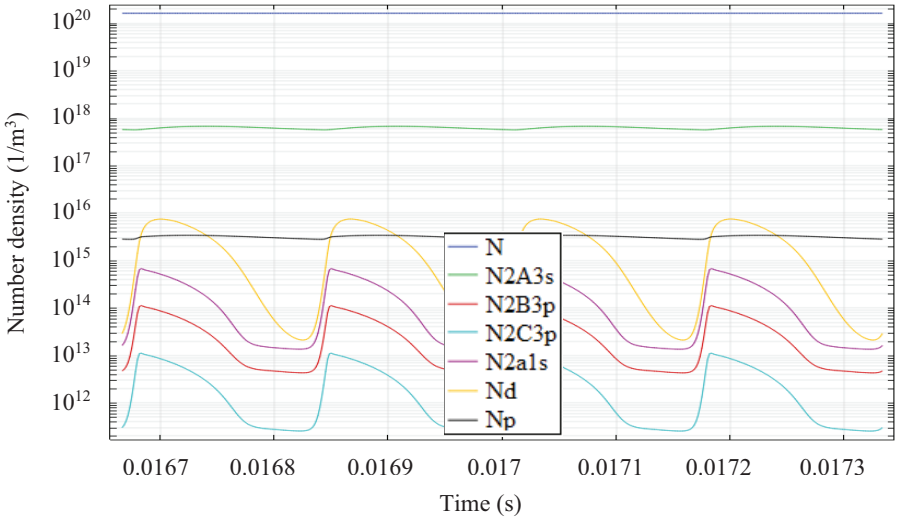

Figure 6. Temporal variation of exited and neutrals species number density.

5. Parametric study

5.1. Dielectric coating effect

Several dielectric materials used in dielectric barrier discharges (DBD) as ceramics (Alumin 96% used in this model), glass, silicon and polymer. These materials have the relative permittivity under 10 ($\varepsilon_r < 10$) which

give an ability to take the thickness of each dielectric coating in order of mm [10]. Figure 7 shows the discharge current variation (Figure 7a), electron density (Figure 7b) and $N_2(A^3\sum_u^+)$ density (Figure 7c) for each dielectric material (Alumina $\varepsilon_r = 9$, Glass $\varepsilon_r = 8.2$, Stumatite $\varepsilon_r = 7.3$). As we observe in Figures 7a–7c, the discharge current is proportional to the relative permittivity while the electron density and the density $N_2(A^3\sum_u^+)$ are almost the same for the three types of dielectric. The change in dielectric materials (relative permittivity ε_r) makes it possible to estimate the density of the plasma (electrons and heavy species) through space and the discharge current.

5.2. Applied voltage effect

To study the effect of the applied voltage on the characteristics of the DBD discharge in nitrogen, we used alumina as dielectric coating material and considered three voltage values, i.e. 4.5, 6, and 8 kV. The influence of the applied voltage on the discharge current, on the electron density and on $N_2(A^3\sum_u^+)$ is shown in Figures 8a–8c, respectively.

According to Dakin et al. [24], breakdown voltage in a gap of 2 mm of thickness filled with nitrogen gas at atmospheric pressure is 8.2 kV. The gap gas of our model has 1 mm of thickness, so as it shown in Figure 8a, that under a voltage of 4.5 kV, there is no breakdown just a streamer discharge (sinusoidal waveform of current). Discharge current increase with voltage, and the displacement current get shorter period.

From Figures 8b and 8c, it appears that the density of the electron and the density of $N_2(A^3\sum_u^+)$ are almost the same for V = 6 kV and V = 8 kV on the anode side, the density of metastables has minimum values between electrodes (0.5 mm), whereas with V = 4.5 kV in this position, there are fewer metastable species (15 * $10^{18}/\mathrm{m}^3$ approximately)

5.3. Frequency effect

This section shows the influence of applied voltage frequency on discharge current (Figure 9a), electron density (Figure 9b) and $N_2(A^3\sum_u^+)$ density (Figure 9c). As it is shown in this figure, the waveform does not change, but the peak of current increase with frequency.

Also, we can see that the electron density undergoes a slight change in space, while the density $N_2(A^3\sum_u^+)$ at 3 kHz is greater than the density at 5 kHz and 7 kHz near the anode. Increasing the frequency makes the ionization of the particles weaker, so there are less $N_2(A^3\sum_u^+)$ particles near the anode at 7 kHz.

6. Modeling of the double dielectric reactor

6.1. Model description

In this part of our work, we consider a DBD reactor whose dielectric coating materials of the two electrodes are different.

By using the three types of dielectric coating materials mentioned previously in this article (Alumina $\varepsilon_r = 9$, Glass $\varepsilon_r = 8.2$ and Stumatite$\varepsilon_r = 7.3$), we obtain three case studies shown in Figure 10.

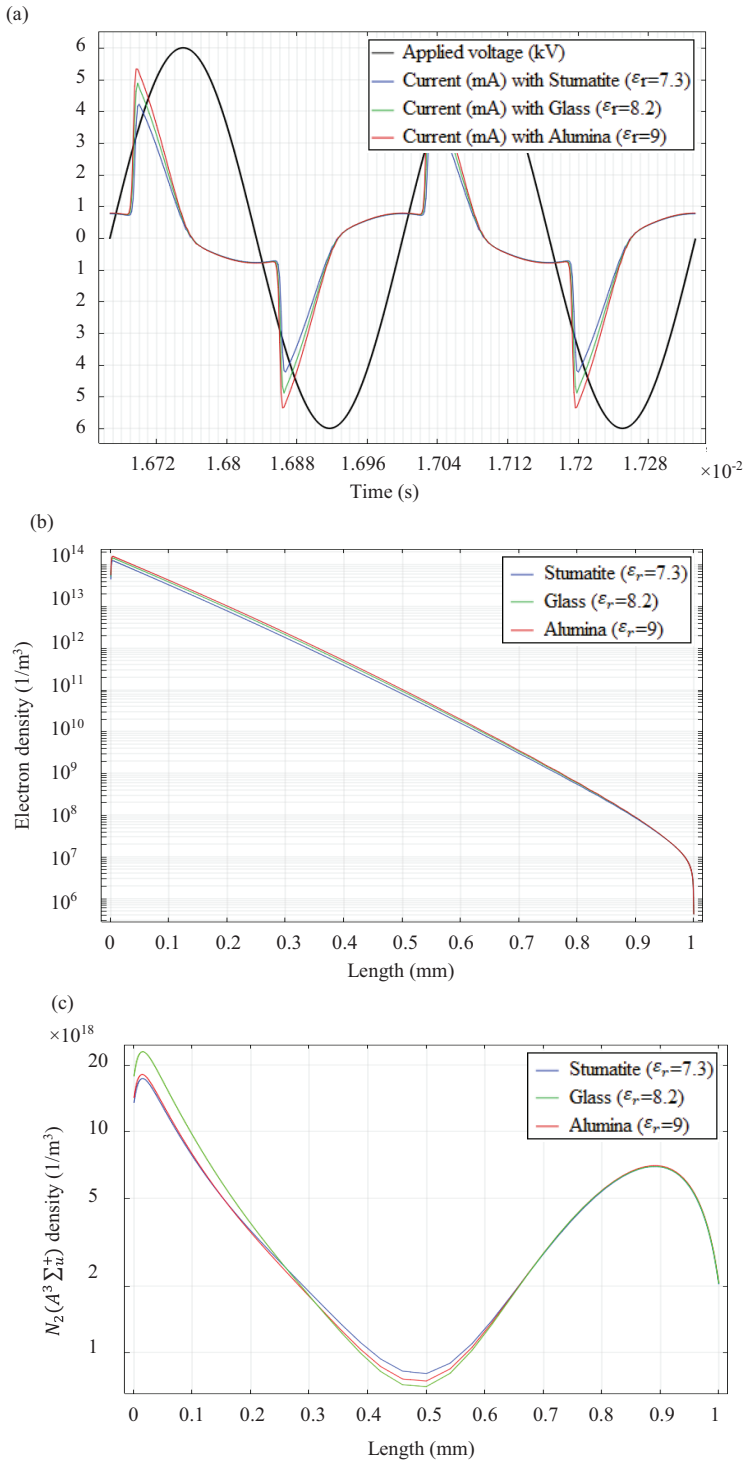

Figure 7. Effect of dielectric coating materials on: (a) discharge current, (b) electron density, (c) $N_2(A^3\sum_u^+)$ density.

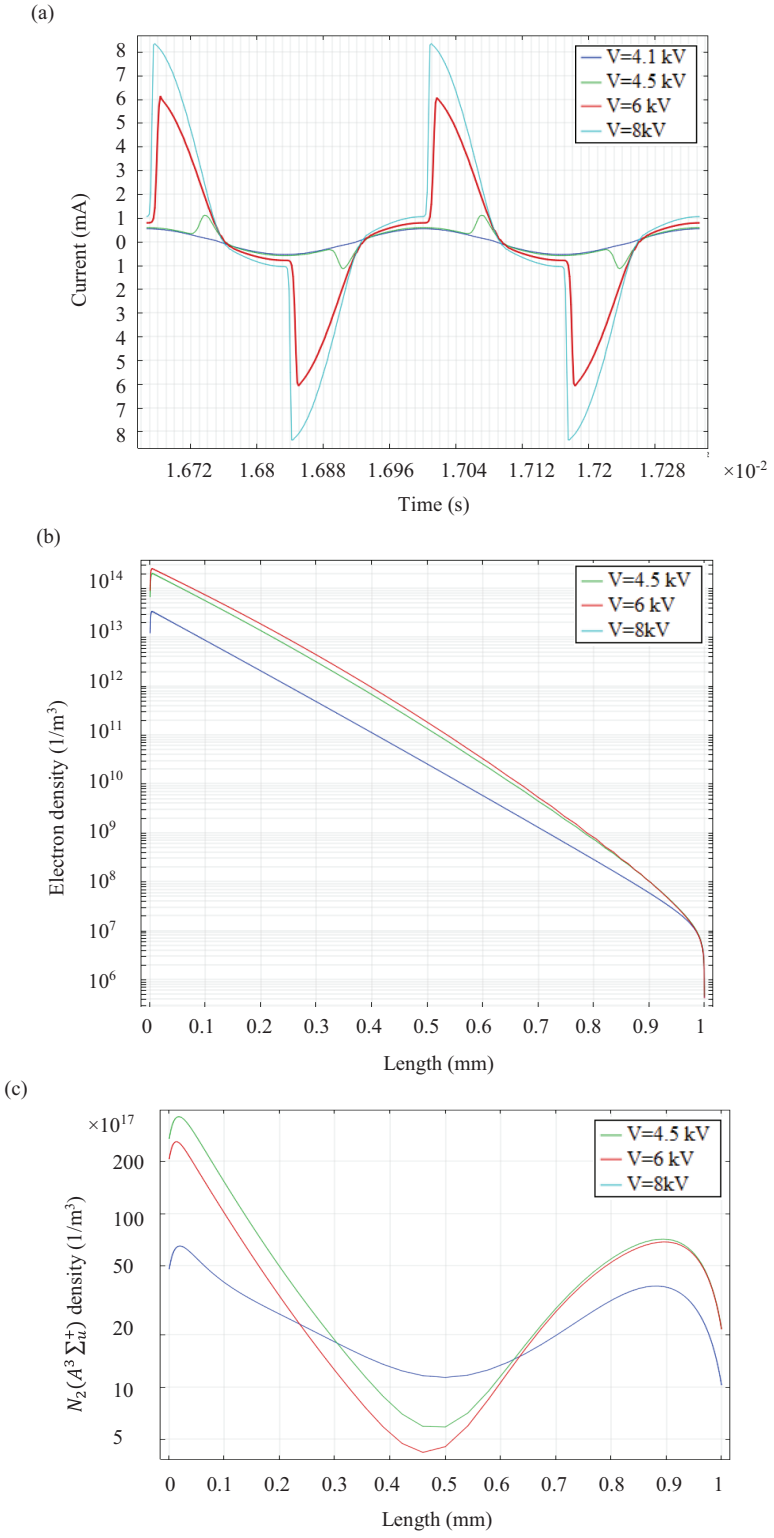

Figure 8. Effect of applied voltage on: (a) discharge current, (b) electron density, (c) $N_2(A^3\sum_u^+)$ density.

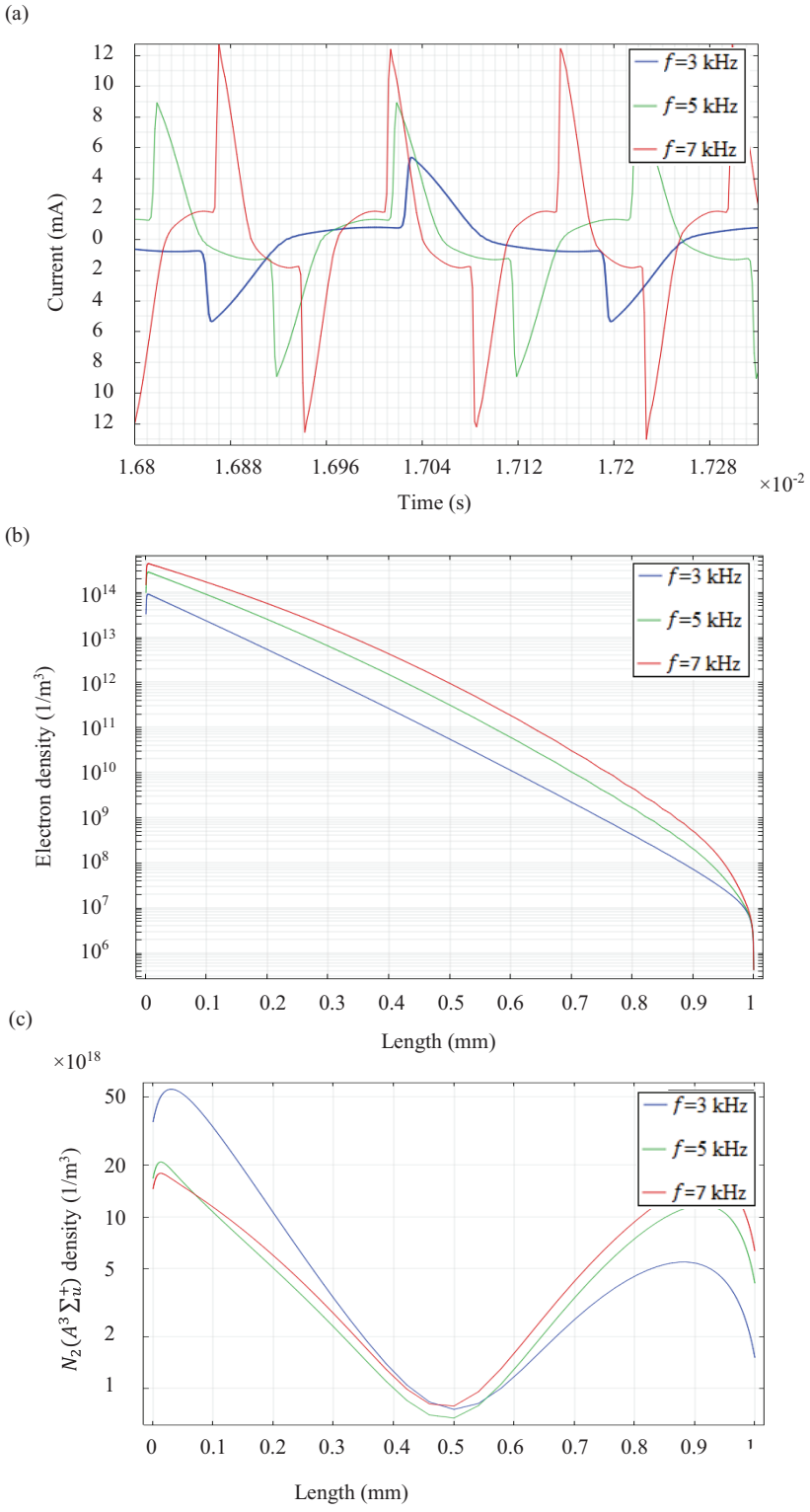

Figure 9. Effect of frequency on: (a) discharge current, (b) electron density, (c) $N_2(A^3\sum_u^+)$ density.

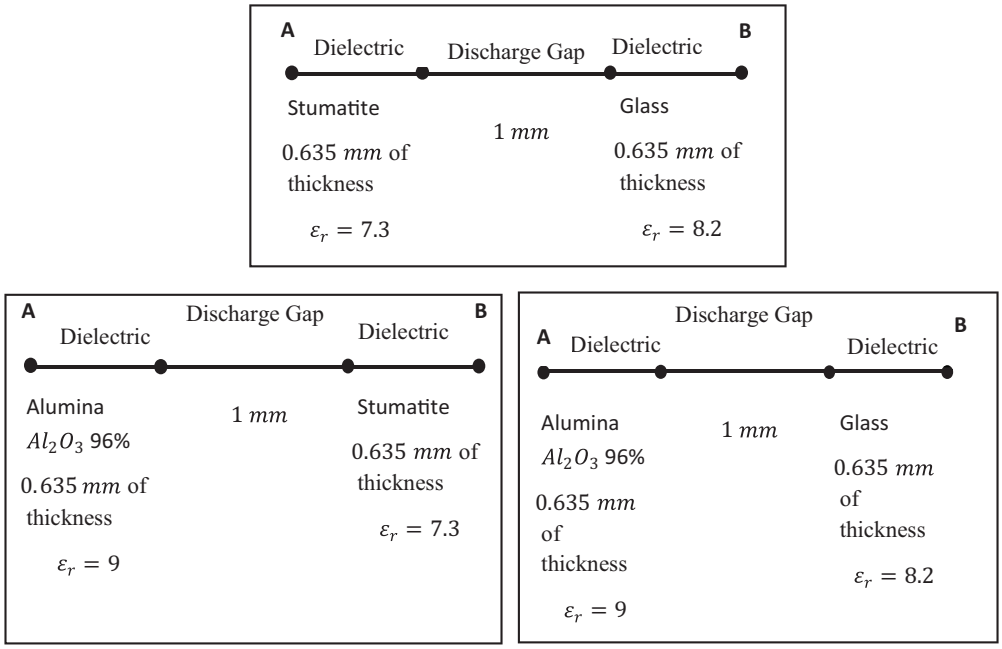

Figure 10. Geometry of the three cases studied for the double dielectric reactor.

6.2. Simulation results

Figures 11 and 12, respectively, show a comparison between the discharge currents and the plasma densities in the three types of DBD reactor. Figure 11 shows that all the forms of current are identical, the difference between them lies in the current peak due to the variation of the equivalent capacitor of the dielectrics.

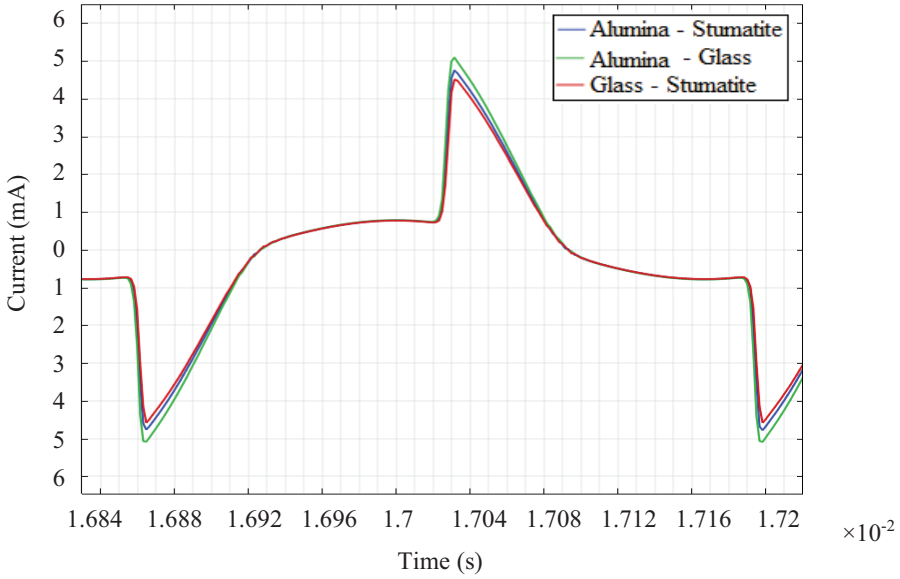

Figure 11. Discharge current in the three types of DBD reactors considered.

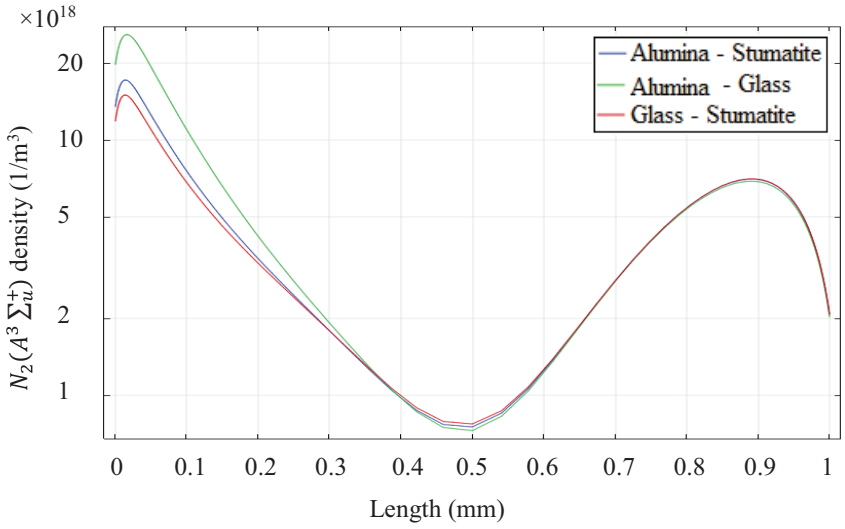

Figure 12. $N_2(A^3\sum_u^+)$ density in the three types of DBD reactors considered.

For the plasma density ($N_2(A^3\sum_u^+)$, we also get almost identical shapes near the grounded electrode for the three types of DBD reactor, but a small difference in values is recorded near the high voltage electrode at a distance of approximately 0.05 mm.

7. Conclusion

Our work aimed to study by simulation the dielectric barrier discharge (DBD) in pure nitrogen at atmospheric pressure in 1D parallel-plate geometry, driven by a sinusoidal voltage power source using a self-consistent fluid model considering the local average energy approximation. The simulated discharge currents obtained are in very good agreement with the experimental measurements. All the nitrogen reactions have led to an interpretation of the behavior of 13 species present in the plasma with regard to the evolution in space and time. The parametric study carried out on some parameters of the DBD has proved that the discharge current is proportional to the relative permittivity while the electron density and the density $N_2(A^3\sum_u^+)$ are about the same for the types of dielectrics considered, thus, the discharge current increases with the voltage and the displacement current becomes shorter. Also, the waveform of the discharge current does not change but the peak current increases with the frequency value. This section approves that by manipulating each of these parameters, it can optimize the discharge current or density of the plasma.

References

[1] Jeongy JY, Babayany SE, Tuy VJ, Parkz J, Heninsy I et al. Etching materials with anatmospheric-pressure plasma jet. Plasma Sources Science and Technology 1998; 7: 282-285.

[2] Choi YH, Kim JH, Hwang YS. One-dimensional discharge simulation of nitrogen DBD atmospheric pressure plasma .Thin Solid Films 2006; 506-507: 389-395.

[3] Massines F, Segur P, Gherardi N, Khamphan C, Ricard A. Physics and chemistry in a glow dielectric barrier discharge at atmospheric pressure: diagnostics and modelling. Surface and Coatings Technology 2003; 174: 8-14.

[4] Panousis E, Papageorghiou L, Spyrou N, Loiseau JF, Held B. Numerical modelling of an atmospheric pressure dielectric barrier discharge in nitrogen: electrical and kinetic description. Journal Physics D: Applied Physics 2007; 40: 4168-4180.

[5] Cheng KW, Hung CT, Lin KM, Chiu YM, Wu JS et al. Fluid modeling of a nitrogen atmospheric-pressure planar dielectric barrier discharge driven by a realistic distorted sinusoidal alternating current power source. Japanese Journal of Applied Physics 2012; 51: 11600.

[6] Braun D, Gibalovt V, Pietsch G. Two-dimensional modelling of the dielectric barrier discharge in air. Plasma Sources Science and. Technology 1992; 7: 166-174.

[7] Kogelschatz U. Atmospheric-pressure plasma technology. Plasma Physics Controlled Fusion 2004; 46: B63-B75.

[8] Mazouffre S, Foissac C, Supiot P, Vankan P, Engeln R et al. Density and temperature of N atoms in the afterglow of a microwave discharge measured by a two-photon laser-induced ?uorescence technique. Plasma Sources Science and Technology 2001; 10: 168-175.

[9] Bouzidi MC, Bonnin X, Naudé N, Piquet H, Belinger A et al. Maximization of the working domain of an atmospheric pressure Townsend discharge (APTD) using a current-source static converter. Journal of Physics: Conference Series 2014; 550: 012044.

[10] Prevosto L, Kelly H, Mancinelli B. Modelling of an atmospheric pressure nitrogen glow discharge operating in high-gas temperature regimes. Plasma Chemistry and Plasma Processing 2016; 36: 973-992.

[11] Gadkari S, Tu X , Gu S. Fluid model for a partially packed dielectric barrier discharge plasma reactor. Physics of Plasmas 2017; 24: 093510.

[12] Hagelaar GJM, Pitchford LC. Solving the Boltzmann equation to obtain electron transport coefficients and rate coefficients for fluid models. Plasma Sources Science and Technology 2005;14: 722-733.

[13] Ghassemi M, Mohseni H, Niayesh K, Shayegani AA. Dielectric barrier discharge (DBD) dynamic modeling for high voltage insulation. In: Electrical Insulation Conference; Annapolis, MD, USA; 2011. pp. 156-161.

[14] Boeuf JP, Pitchford LC. Two-dimensional model of a capacitively coupled rf discharge and comparisons with experiments in the gaseous electronics conference reference reactor. Physical Review E 1995; 51 (2): 1376-1390.

[15] Wei LS, Peng BF, Li M, Zhang YF. A numerical study of species and electric ?eld distributions in pulsed DBD in oxygen for ozone generation. Vacuum 2016; 125: 123-132.

[16] Tanvir F, Bakhtier F, Staack D, Gutsol A, Fridman A. Simulation of dc atmospheric pressure argon micro glow-discharge. Plasma Sources Science and Technology 2006; 15: 676-688.

[17] Peterson JR, Le Padellec A, Danared H, Dunn GH, Larsson M et al. Dissociative recombination and excitation of $N_2{}^+$: cross sections and product branching ratios. The Journal of Chemical Physics 1998; 5: 108.

[18] Bacri J, Medani A. Electron diatomic molecule weighted total cross section calculation. Physica 1982;112C: 101-l 18.

[19] Kossyi IA, Kostinsky AY, Matveyev AA, Silakov VP. Kinetic scheme of the non-equilibrium discharge in nitrogen-oxygen mixtures. Plasma Sources Science and Technology 1992; 1: 207-220.

[20] Lazarou C, Koukounis D, Chiper AS, Costin C, Topala I et al. Numerical modeling of the effect of the level of nitrogen impurities in a helium parallele plate dielectric barrier discharge. Plasma Sources Science and Technology 2015; 24 (13): 035012.

[21] Tsai H, Hsu C. Numerical simulation of downstream kinetics of an atmospheric-pressure nitrogen plasma jet. IEEE Transactions on Plasma Science 2010; 38: 12.

[22] Moseley ZT, Snuggs RM, Martin DW, McDaniel EW. Nobilities, diffusion coefficients, and reaction rates of mass-indentified nitrogen ions in nitrogen. Pphysical Review 1969; 178: 240.

[23] Ellis HW, Pai RY, McDaniel EW. Transport properties of gaseous ions over a wide energy range. Atomic Data And Nuclear Data Tables 1976; 17: 177-210.

[24] Dakin TW, Luxa G, Oppermann G,Vigreux J, Wind G et al. Electra 1974; 32: 61-82.